

Article

Trajectory Linearization-Based Adaptive PLOS Path Following Control for Unmanned Surface Vehicle with Unknown Dynamics and Rudder Saturation

Bingbing Qiu , Guofeng Wang * and Yunsheng Fan 

Marine Electrical Engineering College, Dalian Maritime University, Dalian 116026, China; bbqiu.dmu@gmail.com (B.Q.); yunsheng@dlmu.edu.cn (Y.F.)

* Correspondence: gfwangsh@163.com; Tel.: +86-0411-8472-5623

Received: 9 April 2020; Accepted: 18 May 2020; Published: 20 May 2020



Abstract: This paper presents a novel robust control strategy for path following of an unmanned surface vehicle (USV) suffering from unknown dynamics and rudder saturation. The trajectory linearization control (TLC) method augmented by the neural network, linear extended state observer (LESO), and auxiliary system is used as the main control framework. The salient features of the presented strategy are as follows: in the guidance loop, a fuzzy predictor line-of-sight (FPLOS) guidance law is proposed to ensure that the USV effectively follows the given path, where the fuzzy method is introduced to adjust lookahead distance online, and thereby achieving convergence performance; in the control loop, we develop a practical robust path following controller based on enhanced TLC, in which the neural network and LESO are adopted to handle unmodeled dynamics and external disturbances, respectively. Meanwhile, a nonlinear tracking differentiator (NTD) is constructed to achieve satisfactory differential and filter performance. Then, the auxiliary system is incorporated into the controller design to handle rudder saturation. Using Lyapunov stability theory, the entire system is ensured to be uniformly ultimately bounded (UUB). Simulation comparisons illustrate the effectiveness and superiority of the proposed strategy.

Keywords: path following; TLC method; LESO; predictor line-of-sight; fuzzy method; neural network; NTD

1. Introduction

In recent years, unmanned surface vehicles (USV) have received significant attention, due to their broad applications in the marine environment, such as ocean surveillance, gas exploration, and marine transportation [1–3]. In these applications, the high tracking performance and complex external environment make the USV path following control challenging.

Path following is a motion control scenario where the USV has to follow a predefined path without a temporal constraint [4–6]. At present, various control methods have been proposed in the literature. In [7], an adaptive control approach based on the backstepping technique was developed for an unmanned marine surface vessel, which was also suitable for other unmanned vehicles. Using the dynamic surface control (DSC) method, a practical path following control scheme was developed for underactuated ships in [8], whose advantage was that it could deal with the practical condition “waypoints based navigation”. The paper [9] presented an effective control approach for path following of marine vehicles, where the input-output feedback linearization method being applied by defining “hand position” as the output. In addition, a popular and effective guidance method adopted in path following is line-of-sight (LOS) guidance [10–13]. The main idea is to implement a lookahead based LOS guidance law mimicking a helmsman and generate a desired heading angle, which is fed into the

inner dynamics loop. In [14], an integral LOS (ILOS) guidance law based on monotone cubic Hermite interpolation was developed, and the main innovation was that it proposed a time-varying equation for the lookahead distance. In [15], a novel guidance control method was presented for a marine surface vehicle (MSV), in which the unknown sideslip angle was estimated using a reduced-order ESO. The paper [16] proposed a sideslip-tangent LOS (SLOS) guidance strategy, where the sideslip angle was eliminated by constructing a finite-time sideslip observer (FSO). Compared with [14,15], the advantage was that it could handle a large sideslip angle. The paper [17] proposed an adaptive LOS (ALOS) algorithm for unmanned aerial vehicles, in which an adaptive law was constructed to handle the unknown sideslip angle.

On the other hand, in order to deal with complex interference, scholars have put forward many excellent solutions [18,19]. A concise path following controller was designed for a podded propulsion USV in [20], in which unmodeled dynamics and disturbances were handled by introducing the neural network minimum parameter learning method. The paper [21] proposed a robust compound control method subject to bounded uncertainties, where LESO was used to estimate the system uncertainties. A novel sigmoid function based disturbance observer was designed to eliminate various uncertainties effectively in [22], which was proven to be an efficient observer. The paper [23] developed an online constructive fuzzy approximator by the decoupled structure learning mechanism, which was incorporated into the dominant adaptive controller to identify unknown nonlinearities and unknown external disturbances exactly. Besides, input saturation [24,25] is common and inevitable, which may lead to system instability. In [26], a path following controller was presented for a surface vessel, in which the auxiliary system developed could cope very well with input saturation without any downtime. Considering disturbances and input saturation, the paper [27] addressed the course tracking problem of ships, where the rudder saturation was compensated using an auxiliary dynamic system. The paper [28] developed a novel trajectory tracking control method, in which a Gaussian error function was introduced to approximate input saturation.

Motivated by the above observations, considering unknown dynamics, disturbances, and rudder saturation, this article presents a novel path following control strategy for the USV. This paper covers the following three contributions:

- (1) An improved PLOS guidance law is constructed to calculate the desired heading angle and estimate unknown sideslip angle. Compared with [13], a fuzzy method is incorporated into the proposed PLOS guidance law to optimize the lookahead distance, thus achieving better convergence quality.
- (2) As a new control method in the USV motion control field, an enhanced TLC is adopted to design a concise path following controller for USV. Compared with traditional TLC, the enhanced TLC only needs one parameter to be adjusted.
- (3) Both unknown dynamics and disturbances can be estimated by constructing a neural network and LESO, respectively, and the rudder saturation is effectively resolved by using an auxiliary system.

The structure of this paper is as follows. The problem formulation and preliminaries are introduced in Section 2. Section 3 presents a novel control strategy for the USV. Stability analysis is given in Section 4. Section 5 is the simulation result verification. Finally, Section 6 gives the conclusions and future works.

2. Problem Formulation and Preliminaries

Notations: $|\bullet|$ represents the absolute operator. $\|\bullet\|$ represents the Euclidean norm. $\hat{\bullet}$ denotes the estimate value. $\tilde{\bullet} = \hat{\bullet} - \bullet$ denotes the error.

2.1. USV Model

In this section, we first define the frames: the Earth-fixed inertial frame X_0OY_0 (i) and the body-fixed frame X_pOY_p (b), as illustrated in Figure 1. Then, we only consider the horizontal motion of the USV, namely, neglecting roll p , pitch q , and heave w .

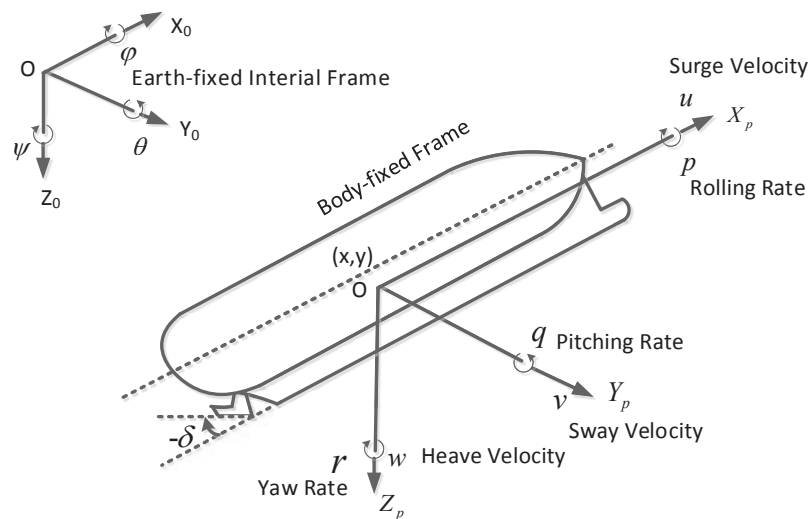


Figure 1. The Earth-fixed inertial and the body-fixed frame.

From [17], the kinematic equation of the USV can be modeled by:

$$\begin{cases} \dot{x} = u \cos \psi - v \sin \psi \\ \dot{y} = u \sin \psi + v \cos \psi \\ \dot{\psi} = r \end{cases} \quad (1)$$

where (x, y, ψ) is the position and orientation of the USV in (i) and u, v , and r include the frame (b) surge, sway, and yaw velocities, respectively.

Considering the actual situation of USV navigation, the Norrbinn nonlinear model [27] with respect to USV steering control is given by:

$$\begin{cases} \dot{\psi} = r \\ \dot{r} = -\frac{1}{T}r - \frac{\alpha}{T}r^3 + \frac{K}{T}\delta \end{cases} \quad (2)$$

where δ is the rudder angle, α is the Norrbinn coefficient, T is the time constant, and K is the gain constant.

Combining the system (1) and (2), the nonlinear mathematical model of the USV is written as:

$$\begin{cases} \dot{x} = u \cos \psi - v \sin \psi \\ \dot{y} = u \sin \psi + v \cos \psi \\ \dot{\psi} = r \\ \dot{r} = f(r) + \Delta f(r) + b\mu + d \\ y_1 = x \\ y_2 = y \end{cases} \quad (3)$$

where $f(r) = -\frac{1}{T}r - \frac{\alpha}{T}r^3$, $b = \frac{K}{T}$, and y_1, y_2 denote the output signal; $\Delta f(r), d$ represent unknown dynamics and multiple disturbances, respectively. $\mu = \delta$ is the input of the USV. Considering the saturation characteristics of the rudder, it can be described as:

$$\mu = \begin{cases} \mu_{\max}, & \text{if } \mu_0 > \mu_{\max} \\ \mu_0, & \text{if } \mu_{\min} \leq \mu_0 \leq \mu_{\max} \\ \mu_{\min}, & \text{if } \mu_0 < \mu_{\min} \end{cases} \quad (4)$$

where μ_{\max} and μ_{\min} represent the amplitudes of input saturation. From [29], we know $\mu_{\max} = 35^\circ$, $\mu_{\min} = -35^\circ$.

Remark 1. Here, the frequency of d is low compared to the USV dynamics, and it is also filtered by a nonlinear tracking differentiator. Hence, d is considered to be slow time-varying disturbance [30].

Our control objective is to design a robust adaptive path following control strategy with completely unknown dynamics, disturbances, and rudder saturation, so that the USV tracks the reference path (x_d, y_d) with an arbitrarily small error.

2.2. Preliminaries

Assumption 1. The multiple disturbances are bounded with $|d| \leq d_{\max}$, where d_{\max} is unknown positive constant.

Lemma 1 ([31]). Considering following system:

$$\dot{X} = A_c(t) X \quad (5)$$

where A_c is continuous and bounded. Let $Q_1(t)$ be a bounded, positive, symmetric matrix, such as $0 < \lambda_3 I \leq Q(t) \leq \lambda_4 I$. There exists a symmetric matrix $P(t)$ meeting:

$$A_c^T(t) P(t) + P(t) A_c(t) + \dot{P}(t) + Q(t) = 0 \quad (6)$$

where $P(t) = \int_t^\infty \tilde{h}^T(\iota, t) Q(\iota) \tilde{h}(\iota, t) d\iota$, $\|\tilde{h}(\iota, t)\| \leq o_1 e^{-o_2(\iota-t)}$, $0 < \lambda_1 I \leq P(t) \leq \lambda_2 I$.

Trajectory linearization control (TLC) [32–35]: TLC has proven to be an effective robust control method, whose structure is shown in Figure 2. It is clearly noticed that TLC consists of an open-loop dynamic inversion and a linear time-varying (LTV) feedback regulator, in which the dynamic inversion transforms the tracking problem into a time-varying nonlinear tracking error adjustment problem, and the LTV regulator achieves robust stability and performance along the nominal trajectory. Hence, TLC produces robust stability and anti-interference ability, for which TLC has been widely applied to a model-scaled helicopter [33], a 6DOF aircraft [34], and a car-like ground vehicle [35]. However, TLC is rarely used in the control of a USV.

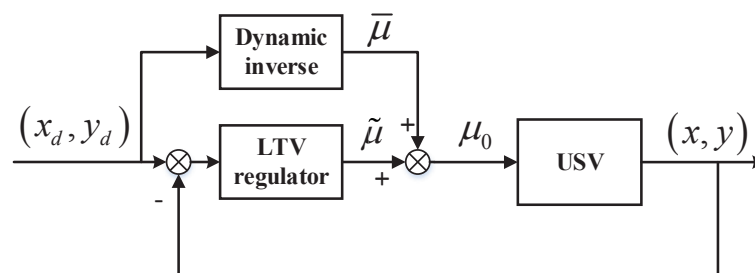


Figure 2. TLC scheme diagram.

Neural network: For unknown continuous function $\Delta f(X)$ ($\mathbb{R}^m \rightarrow \mathbb{R}$), it can be approximated over a compact set $\Phi_X \subseteq \mathbb{R}^m$ with the following radial basis function neural network (RBFNN):

$$\Delta f(X) = W^{*T}S(X) + \varepsilon \tag{7}$$

where $X \in \Phi_X$ denotes the input, $W^* \in \mathbb{R}^l$ denotes the ideal weight, and l is the node number. From [36], we know that the number of NN nodes determines the approximation ability, and the ideal weight vector is written as:

$$W^* = \arg \min_{\hat{W}} \left\{ \sup_{X \in \Psi_X} \left| \Delta f(X) - \hat{W}^T S(X) \right| \right\} \tag{8}$$

$S(X) = [S_1(X), \dots, S_l(X)]^T$ represents the RBF vector, which is defined by:

$$S_i(X) = \exp \left(-\frac{\|X - \rho_i\|^2}{2h_i^2} \right), i = 1, \dots, l \tag{9}$$

where ρ_i and h_i are the center and spread, respectively, and the approximation error ε is bounded with $|\varepsilon| \leq \bar{\varepsilon}$, where $\bar{\varepsilon}$ is unknown positive constant.

3. Path Following Control Strategy

3.1. Structure of the Proposed Control Strategy

A novel path following control strategy is shown in Figure 3. We can see from Figure 3 that it consists mainly of the fuzzy predictor line-of-sight (FPLOS) guidance and the composite control strategy. The proposed FPLOS guidance strategy can not only provide the desired heading angle, but also compensate for the unknown sideslip angle. The proposed composite control strategy consists of two parts: the first part is that TLC controller ensures that the actual heading tracks the guidance heading; the second part is that the compensation controller is capable of solving unmodeled dynamics, multiple disturbances, and rudder saturation by using the NN, reduced-order LESO, and auxiliary system, respectively. Meanwhile, a nonlinear tracking differentiator (NTD) provides a satisfactory differentiation and filtering effect. In the control loop, μ_m , μ_l , and μ_n represent the outputs of NN, LESO, and auxiliary system, respectively; μ_r is a robust term.

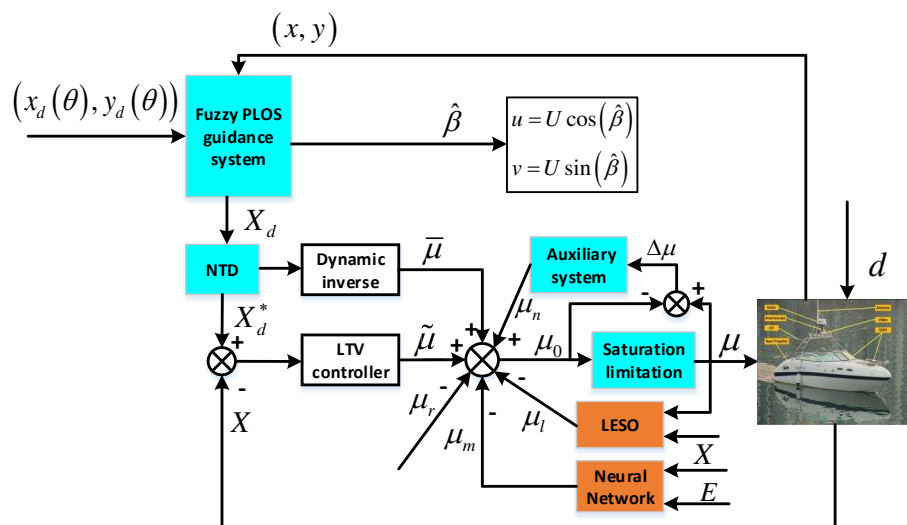


Figure 3. The block diagram of the proposed control strategy for the USV.

3.2. Guidance System Design

In this section, a predictor is used to estimate the unknown sideslip angle induced by wind, waves, and currents. Then, an FPLOS guidance law is proposed, where the lookahead distance is optimized using the fuzzy method.

3.2.1. Estimation of Sideslip Angle

As is illustrated in Figure 4, consider that the desired continuous path $(x_d(\theta), y_d(\theta))$ to be tracked is parameterized by a path variable θ . Then, the path-tangential angle ϕ_p is given by:

$$\phi_p(\theta) = \text{atan2}(y'_d(\theta), x'_d(\theta)) \tag{10}$$

where $x'_d(\theta) = \partial x_d / \partial \theta$ and $y'_d(\theta) = \partial y_d / \partial \theta$.

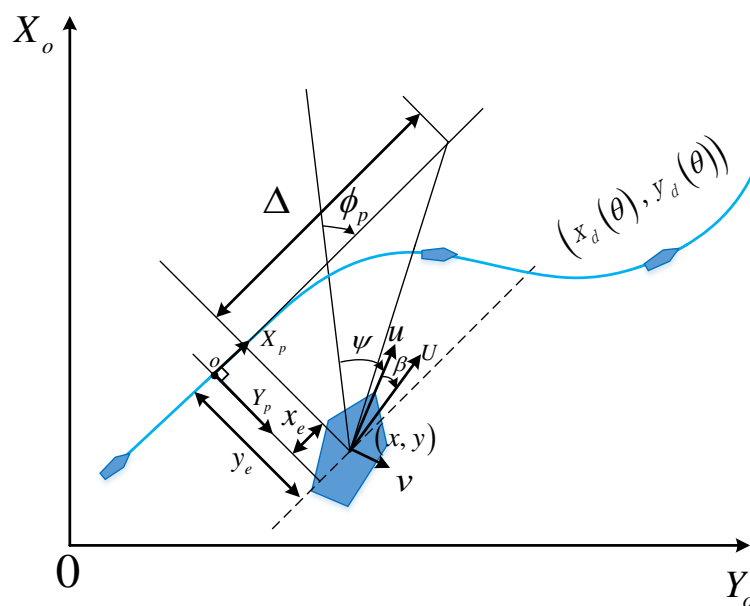


Figure 4. Geometrical illustration of LOS guidance.

For the USV located at (x, y) , the errors x_e and y_e in X_pOY_p are written as:

$$\begin{bmatrix} x_e \\ y_e \end{bmatrix} = \begin{bmatrix} \cos \phi_p & -\sin \phi_p \\ \sin \phi_p & \cos \phi_p \end{bmatrix}^T \begin{bmatrix} x - x_d(\theta) \\ y - y_d(\theta) \end{bmatrix} \tag{11}$$

where y_e and x_e denote cross- and along-track errors, respectively.

Calculating the derivative of (11) along (1) yields:

$$\begin{aligned}
 \dot{x}_e &= u \cos(\psi - \phi_p) - v \sin(\psi - \phi_p) \\
 &\quad + \dot{\phi}_p \underbrace{[-(x - x_d) \sin \phi_p + (y - y_d) \cos \phi_p]}_{y_e} \\
 &\quad - \dot{\theta} \sqrt{x'_d{}^2 + y'_d{}^2} \cos(\phi_p + \varphi) \\
 &= U \cos(\psi - \phi_p) \cos \beta - U \sin(\psi - \phi_p) \sin \beta \\
 &\quad + \dot{\phi}_p y_e - u_p \\
 \dot{y}_e &= u \sin(\psi - \phi_p) + v \cos(\psi - \phi_p) \\
 &\quad - \dot{\phi}_p \underbrace{[-(x - x_d) \cos \phi_p + (y - y_d) \sin \phi_p]}_{x_e} \\
 &= U \sin(\psi - \phi_p) \cos \beta + U \cos(\psi - \phi_p) \sin \beta \\
 &\quad - \dot{\phi}_p x_e
 \end{aligned} \tag{12}$$

where $U = \sqrt{u^2 + v^2} > 0$, $0 < U_{\min} \leq U \leq U_{\max}$, and $\beta = \text{atan2}(v, u)$ denotes the sideslip angle. u_p is the virtual target speed to stabilize x_e , which is selected as:

$$u_p = \dot{\theta} \sqrt{x'_d{}^2(\theta) + y'_d{}^2(\theta)} \tag{13}$$

Note that the sideslip angle is relatively small in practice [25], and we have:

$$\begin{cases} \dot{x}_e = U \cos(\psi - \phi_p) - U \sin(\psi - \phi_p) \beta + \dot{\phi}_p y_e - u_p \\ \dot{y}_e = U \sin(\psi - \phi_p) + U \cos(\psi - \phi_p) \beta - \dot{\phi}_p x_e \end{cases} \tag{14}$$

In order to exactly compensate for the unknown sideslip angle, two predictors are developed as:

$$\begin{cases} \dot{\hat{x}}_e = U \cos(\psi - \phi_p) - U \sin(\psi - \phi_p) \hat{\beta} + \dot{\phi}_p y_e - u_p - k_x \tilde{x}_e \\ \dot{\hat{y}}_e = U \sin(\psi - \phi_p) + U \cos(\psi - \phi_p) \hat{\beta} - \dot{\phi}_p x_e - k_y \tilde{y}_e \end{cases} \tag{15}$$

where k_x and k_y are the design parameters, $\tilde{x}_e = \hat{x}_e - x_e$, $\tilde{y}_e = \hat{y}_e - y_e$ are the prediction errors, and $\hat{\beta}$ is the estimation of β . The corresponding adaptive updating law is selected as:

$$\dot{\hat{\beta}} = \gamma [U \sin(\psi - \phi_p) \tilde{x}_e - U \cos(\psi - \phi_p) \tilde{y}_e] \tag{16}$$

The, \tilde{x}_e , \tilde{y}_e , and $\tilde{\beta}$ are written as:

$$\begin{cases} \dot{\tilde{x}}_e = -U \sin(\psi - \phi_p) \tilde{\beta} - k_x \tilde{x}_e \\ \dot{\tilde{y}}_e = U \cos(\psi - \phi_p) \tilde{\beta} - k_y \tilde{y}_e \\ \dot{\tilde{\beta}} = \gamma [U \sin(\psi - \phi_p) \tilde{x}_e - U \cos(\psi - \phi_p) \tilde{y}_e] \end{cases} \tag{17}$$

Theorem 1. The proposed update law (16) makes the errors \tilde{x}_e and \tilde{y}_e to converge to origin, thus ensuring that the system (17) is uniformly asymptotically stable (UAS).

Proof of Theorem 1. Define the Lyapunov function by:

$$V_1 = \frac{1}{2} \tilde{x}_e^2 + \frac{1}{2} \tilde{y}_e^2 + \frac{1}{2} \gamma^{-1} \tilde{\beta}^2 \tag{18}$$

Differentiating V_1 along (16) and (17) yields:

$$\begin{aligned} \dot{V}_1 &= \tilde{x}_e (-U \sin(\psi - \phi_p) \tilde{\beta} - k_x \tilde{x}_e) + \tilde{y}_e (U \cos(\psi - \phi_p) \tilde{\beta} - k_y \tilde{\beta}) \\ &\quad + \tilde{\beta} (U \sin(\psi - \phi_p) \tilde{x}_e - U \cos(\psi - \phi_p) \tilde{y}_e) \\ &\leq -k_x \tilde{x}_e^2 - k_y \tilde{y}_e^2 \end{aligned} \tag{19}$$

Hence, we know that the system (17) is UAS. \square

3.2.2. FPLOS Guidance Law

Then, the FPLOS guidance law is given by:

$$\psi_d = \phi_p + \arctan\left(-\frac{\hat{y}_e}{\Delta} - \hat{\beta}\right) \tag{20}$$

where Δ is the user-specified lookahead distance.

Remark 2. Different from the existing LOS guidance in [15,20], Δ of this paper changes with the movement of the USV. The greatest advantage of this proposed guidance strategy is to optimize Δ through the fuzzy method, thereby producing an aggressive behavior to decrease y_e faster. Here, the inputs of the designed fuzzy system are y_e and \dot{y}_e , and the output is Γ . the lookahead distance Δ is designed as $\Delta = \Delta_{\min} + \Gamma (\Delta_{\max} - \Delta_{\min})$.

The velocity u_p is designed to stabilize x_e as the virtual input, which is determined by:

$$u_p = U \cos(\psi - \phi_p) - U \sin(\psi - \phi_p) \hat{\beta} + k_1 \hat{x}_e \tag{21}$$

where k_1 denotes a positive constant.

From (13) and (21), the update law θ can be described by:

$$\dot{\theta} = \frac{U \cos(\psi - \phi_p) - U \sin(\psi - \phi_p) \hat{\beta} + k_1 \hat{x}_e}{\sqrt{x'_d{}^2(\theta) + y'_d{}^2(\theta)}} \tag{22}$$

Based on the above analysis, (15) can be rewritten as:

$$\begin{cases} \dot{\hat{x}}_e = -k_1 \hat{x}_e + \phi_p \hat{y}_e - k_x \tilde{x}_e \\ \dot{\hat{y}}_e = -c_1 \hat{y}_e - \phi_p \hat{x}_e - k_y \tilde{y}_e \end{cases} \tag{23}$$

where $c_1 = \frac{U}{\sqrt{\Delta^2 + (\hat{y}_e + \Delta \hat{\beta})^2}}$.

Theorem 2. Consider the application of (20) and (22) in the system (23). If we choose $k_1 > \frac{k_x}{2}$, $c_1 > \frac{k_y}{2}$, the errors \hat{x}_e and \hat{y}_e are bounded, and the system (23) is UUB.

Proof of Theorem 2. Design a Lyapunov function as follows:

$$V_2 = \frac{1}{2} \hat{x}_e^2 + \frac{1}{2} \hat{y}_e^2 \tag{24}$$

Differentiating (24) and combining (23) and Young’s inequality [15], one has:

$$\begin{aligned} \dot{V}_2 &= -k_1 \hat{x}_e^2 - c_1 \hat{y}_e^2 - k_x \hat{x}_e \tilde{x}_e - k_y \hat{y}_e \tilde{y}_e \\ &\leq -\left(k_1 - \frac{k_x}{2}\right) \hat{x}_e^2 - \left(c_1 - \frac{k_y}{2}\right) \hat{y}_e^2 + \frac{k_x}{2} \tilde{x}_e^2 + \frac{k_y}{2} \tilde{y}_e^2 \\ &\leq -2\lambda V_2 + \Omega \end{aligned} \tag{25}$$

where $\lambda = \min\left\{k_1 - \frac{k_x}{2}, c_1 - \frac{k_y}{2}\right\}$, $\Omega = \frac{k_x}{2} \tilde{x}_e^2 + \frac{k_y}{2} \tilde{y}_e^2$.

Integrating on both sides of (25) yields:

$$V_2 \leq \left(V_2(0) - \frac{\Omega}{2\lambda}\right) e^{-2\lambda t} + \frac{\Omega}{2\lambda} \tag{26}$$

Obviously, V_2 is eventually bounded by $\frac{\Omega}{2\lambda}$, and the system (23) is UUB. \square

3.3. Composite Control Strategy

3.3.1. TLC Control Design

Define $X = [X_1, X_2]^T = [\psi, r]^T$, $F(X) = [X_2, f(X_2)]^T$, $G_1(X) = [0, b]^T$, $G_2(X) = G_3(X) = [0, 1]^T$, $h(X) = X_1$. We have:

$$\begin{cases} \dot{X} = F(X) + G_2(X) \Delta f(X_1) + G_1(X) \mu + G_3(X) d \\ Y = h(X) \end{cases} \tag{27}$$

In addition, there exist three functions $G_0(X)$, $G_4(X)$, $G_5(X)$, which satisfy: $G_1(X) G_0(X) = G_3(X)$, $G_1(X) G_4(X) = G_2(X)$, $G_3(X) G_5(X) = G_2(X)$.

First, when $\Delta f(X_1) = 0$ and $d = 0$, define the nominal state X_d^* . We obtain:

$$\dot{X}_d^* = F(X_d^*) + G_1(X_d^*) \bar{\mu} \tag{28}$$

where $\bar{\mu}$ denotes the nominal input, and NTD [37] is applied to produce X_d^* and \dot{X}_d^* by X_d , which can be written as:

$$\begin{cases} fh = fhan(X_d^*(k) - X_d(k), \dot{X}_d^*(k), R_1, h_1) \\ X_d^*(k+1) = X_d^*(k) + h_1 \dot{X}_d^*(k) \\ \dot{X}_d^*(k+1) = \dot{X}_d^*(k) + h_1 \cdot fh \end{cases} \tag{29}$$

where R_1 is an acceleration factor and h_1 is the sampling period.

Remark 3. In this paper, NTD can better realize differential and fast convergence performance by the acceleration factor R_1 , thus avoiding unnecessary set-point jump.

Then, $\bar{\mu}$ is calculated by inverting (28). One has:

$$\bar{\mu} = G_1(X_d^*)^\dagger (\dot{X}_d^* - F(X_d^*)) \tag{30}$$

where \dagger denotes the pseudo inverse operator, and it is defined as $P^\dagger = P^T (PP^T)^{-1}$.

Define the tracking error $E = X - X_d^* = [E_1, E_2]^T$, and linearizing the first equation of (27) along the nominal $(X_d^*, \bar{\mu})$ yields:

$$\begin{bmatrix} \dot{E}_1 \\ \dot{E}_2 \end{bmatrix} = A_1(t) \begin{bmatrix} E_1 \\ E_2 \end{bmatrix} + B_1(t) \underbrace{\begin{bmatrix} \tilde{\mu}_{11} \\ \tilde{\mu}_{12} \end{bmatrix}}_{:=\tilde{\mu}} \tag{31}$$

where $A_1(t) = \left(\frac{\partial F}{\partial X} + \frac{\partial G_1}{\partial X} \mu \right) |_{X_d^*, \bar{\mu}}$, $B_1(t) = G_1(X) |_{X_d^*, \bar{\mu}}$, $\tilde{\mu}$ denotes the LTV stabilizing controller.

A proportional-integral (PI) control law is designed to stabilize error, which is expressed as:

$$\underbrace{\begin{bmatrix} \tilde{\mu}_{11} \\ \tilde{\mu}_{12} \end{bmatrix}}_{:=\tilde{\mu}} = -K_{p1} \begin{bmatrix} E_1 \\ E_2 \end{bmatrix} - K_{I1} \begin{bmatrix} \int E_1 dt \\ \int E_2 dt \end{bmatrix} \tag{32}$$

Define the augmented error $E_\Omega = [\int E_1 dt, \int E_2 dt, E_1, E_2]^T$. We have:

$$\dot{E}_\Omega = A_c E_\Omega = \begin{bmatrix} 0_{2 \times 2} & I_{2 \times 2} \\ -B_1 K_{I1} & A_1 - B_1 K_{p1} \end{bmatrix}^T E_\Omega \tag{33}$$

where $0_{2 \times 2}$ and $I_{2 \times 2}$ represent 2×2 the zero matrix and identity matrix, respectively.

To provide local exponential stability, the desired A_c is designed as:

$$A_c = \begin{bmatrix} 0_{2 \times 2} & I_{2 \times 2} \\ \text{diag}(-a_{111}, -a_{121}) & \text{diag}(-a_{112}, -a_{122}) \end{bmatrix}^T \tag{34}$$

where $a_{1j1}, a_{1j2} > 0, j = 1, 2$ are the adjustment according to the pole assignment technique, which satisfy:

$$a_{1j1} = \omega_j^2 \tag{35}$$

$$a_{1j2} = 2\omega_j$$

where ω_j is the bandwidth. Obviously, ω_j becomes the only parameter to be tuned. Then, we have:

$$K_{I1} = -B_1^\dagger \text{diag}(-a_{111}, -a_{121}) \tag{36}$$

$$K_{p1} = -B_1^\dagger (A_1 - \text{diag}(-a_{112}, -a_{122}))$$

Hence, the feedback control law is expressed as:

$$\tilde{\mu} = -K_{p1} E - K_{I1} \int E dt \tag{37}$$

3.3.2. Adaptive Compensation Control Design

Define $\Psi_1 = E_\Omega^T P(t)$, $\Psi_2 = E_\Omega^T P(t) G_{33}$, $\Psi_3 = E_\Omega^T P(t) G_{22}$, $\Psi_4 = E_\Omega^T P(t) G_{11}$, $G_{11} = [0_2, G_1]^T$, $G_{22} = [0_2, G_2]^T$, $G_{33} = [0_2, G_3]^T$. For unknown dynamics, RBFNN with l nodes is employed to approximate $\Delta f(X)$, and the corresponding controller is selected as:

$$\mu_m = G_4(X) v_m \tag{38}$$

where $v_m = \Delta \hat{f}(X) = \hat{W}^T S(X)$. The update law with “ κ -correction” is taken to be:

$$\dot{\hat{W}} = \sigma_1 (\Psi_3 S(X) - \kappa_1 (\hat{W} - W_0)) \tag{39}$$

where σ_1, κ_1 represent positive constants, W_0 is the initial value, \hat{W} is the estimate of W , and the estimation error is $\tilde{W} = \hat{W} - W$.

Then, an LESO [38] is constructed to estimate external disturbance, which can be written as:

$$\begin{cases} \dot{\zeta}_1 = -\omega_1 \zeta_1 - \omega_1^2 X_2 - \omega_1 (f(X_2) + \Delta \hat{f}(X) + b\mu) \\ \hat{d} = \zeta_1 + \omega_1 X_2 \end{cases} \tag{40}$$

where \hat{d} denotes the estimate of d ; the estimate error is $\tilde{d} = \hat{d} - d$; ζ_1 is the state; $\omega_1 > 0$ is the observer gain. Define $\hat{d} = \eta_s$, the compensation controller μ_l is given as $\mu_l = G_0(X) \eta_s$.

Then, a robust term is developed to eliminate the estimation errors of NN and LESO, which is designed as:

$$\mu_r = G_0(X) v_r \tag{41}$$

where $v_r = \hat{\vartheta} \operatorname{sgn}(\Psi_3)$. The corresponding adaptive law is:

$$\dot{\hat{\vartheta}} = \sigma_2 (\Psi_2 - \kappa_2 (\hat{\vartheta} - \vartheta_0)) \tag{42}$$

where σ_2, κ_2 are two positive constants.

In order to handle rudder saturation, the following auxiliary dynamic system is introduced:

$$\dot{\Theta} = \begin{cases} -K_\Theta \Theta - \frac{|\Psi_3 \cdot \Delta \mu| + 0.5 \Delta \mu^2}{|\Theta|^2} \cdot \Theta + \Delta \mu, & |\Theta| \geq \chi_1 \\ 0, & |\Theta| < \chi_1 \end{cases} \tag{43}$$

where Θ is the auxiliary state vector, $\Delta \mu = \mu - \mu_0$, K_Θ is a positive design parameter, and χ_1 is a positive parameter.

Therefore, the total control law is summarized as:

$$\mu_0 = \bar{\mu} + \tilde{\mu} + \mu_n - \mu_r - \mu_m - \mu_l \tag{44}$$

where $\mu_n = K_n \Theta$, and K_n is a positive design parameter.

4. Stability Analysis

Based on the control law of the above design, we have:

$$\begin{aligned} \dot{E}_\Omega &= A_c(t) E_\Omega + o(\bullet) + G_{11}(X) \Delta \mu + G_{22}(X) (f(X_2) - v_m) \\ &+ G_{33}(X) (d - \eta_s - v_r) + G_{11}(X) k_n \Theta \end{aligned} \tag{45}$$

where $o(\bullet)$ is the high order term of Taylor expansion. From [29], it shows that $o(\bullet)$ is bounded, which meets: $\|o(\bullet)\| \leq \ell \|E_\Omega\|^2, \forall \|E_\Omega\| < \varsigma$, and ℓ is the normal number.

Theorem 3. For the controlled system (3), suppose Assumption 1 holds. With the application of control laws (20) and (44), disturbance observer (40), the auxiliary system (43), the adaptive laws (16), (39), and (42), one can appropriately select parameters: $Q(t), k_x, k_y, k_1, R_1, h_1, \omega_1, K_\Theta, K_n, \sigma_j, \kappa_j, \omega_j (j = 1, 2)$, and the tracking errors can converge to a residual set of the origin. Then, the final controlled system is UUB.

Proof of Theorem 3. Select the Lyapunov function:

$$V = V_2 + \frac{1}{2}E_{\Omega}^T P(t) E_{\Omega} + \frac{1}{2}\sigma_1^{-1}\tilde{W}^T \tilde{W} + \frac{1}{2}\sigma_2^{-1}\tilde{\vartheta}^2 + \frac{1}{2}\tilde{d}^2 + \frac{1}{2}\Theta^2 \tag{46}$$

In light of (6), the derivative of V is:

$$\begin{aligned} \dot{V} = & \dot{V}_2 - \frac{1}{2}E_{\Omega}^T Q(t) E_{\Omega} + \Psi_1 o(\bullet) + \Psi_4 \Delta \mu - \tilde{W}^T (\Psi_3 S(X) - \sigma_1^{-1} \dot{\hat{W}}) \\ & + \Psi_2 (G_5(X) \varepsilon + \tilde{d} - \hat{\vartheta} \operatorname{sgn}(\Psi_2)) + \Psi_4 K_n \Theta + \sigma_2^{-1} \tilde{\vartheta} \dot{\hat{\vartheta}} + \tilde{d} \dot{\hat{d}} + \Theta \dot{\Theta} \end{aligned} \tag{47}$$

When $\|G_5(X) \varepsilon + \tilde{d}\| \leq \vartheta$, substituting (39), (40), and (42) into (47) yields:

$$\begin{aligned} \dot{V} \leq & \dot{V}_2 - \frac{1}{2}E_{\Omega}^T Q(t) E_{\Omega} + \Psi_1 o(\bullet) + \Psi_4 \Delta \mu - \tilde{W}^T (\Psi_3 S(X) - \sigma_1^{-1} \dot{\hat{W}}) \\ & - \tilde{\vartheta} (|\Psi_2| - \sigma_2^{-1} \hat{\vartheta}) + \Psi_4 K_n \Theta + \Theta \dot{\Theta} \\ \leq & \dot{V}_2 - \frac{1}{2}E_{\Omega}^T Q(t) E_{\Omega} + \Psi_1 o(\bullet) + \Psi_4 \Delta \mu - \kappa_1 (\hat{W}^T - W^T) (\hat{W} - W_0) \\ & - \kappa_2 (\hat{\vartheta} - \vartheta) (\hat{\vartheta} - \vartheta_0) - (\omega_1^2 - 1) \tilde{d}^2 + \frac{\|\tilde{W}^T S\|^2}{2} + \frac{\tilde{\varepsilon}^2}{2} + \Psi_4 K_n \Theta + \Theta \dot{\Theta} \end{aligned} \tag{48}$$

Using Young’s inequality yields:

$$\begin{aligned} \Psi_4 K_n \Theta & \leq \frac{K_n}{2} |\Psi_4|^2 + \frac{K_n}{2} \Theta^2 \\ -\kappa_1 (\hat{W}^T - W^T) (\hat{W} - W_0) & \leq -\frac{\kappa_1}{2} \|\hat{W}^T - W^T\|^2 + \frac{\kappa_1}{2} \|W - W_0\|^2 \\ -\kappa_2 (\hat{\vartheta} - \vartheta) (\hat{\vartheta} - \vartheta_0) & \leq -\frac{\kappa_2}{2} (\hat{\vartheta} - \vartheta)^2 + \frac{\kappa_2}{2} (\vartheta - \vartheta_0)^2 \end{aligned} \tag{49}$$

Then, (48) can be rewritten as:

$$\begin{aligned} \dot{V} \leq & -\left(k_1 - \frac{k_x}{2}\right) \hat{x}_e^2 - \left(c_1 - \frac{k_y}{2}\right) \hat{y}_e^2 - \frac{1}{2} (\lambda_3 - 2\ell_{\zeta} \lambda_2) \|E_{\Omega}\|^2 \\ & - \frac{\kappa_1}{2} \|\hat{W}^T - W^T\|^2 - \frac{\kappa_2}{2} (\hat{\vartheta} - \vartheta)^2 - (\omega_1^2 - 1) \tilde{d}^2 + \Psi_4 \Delta \mu + \Theta \dot{\Theta} \\ & + \frac{K_n}{2} |\Psi_4|^2 + \frac{K_n}{2} \Theta^2 + \frac{\|\tilde{W}^T S\|^2}{2} + \frac{\tilde{\varepsilon}^2}{2} + \frac{\kappa_1}{2} \|W - W_0\|^2 + \frac{\kappa_2}{2} (\vartheta - \vartheta_0)^2 \\ & + \frac{k_x}{2} \tilde{x}_e^2 + \frac{k_y}{2} \tilde{y}_e^2 \end{aligned} \tag{50}$$

When $|\Theta| \geq \chi_1$, combining (43) and Young’s inequality, one has:

$$\begin{aligned} \Theta \dot{\Theta} & = -K_{\Theta} \Theta^2 - |\Psi_3 \cdot \Delta \mu| - \frac{1}{2} \Delta \mu^2 + \Delta \mu \Theta \\ & \leq -\left(K_{\Theta} - \frac{1}{2}\right) \Theta^2 - |\Psi_3 \Delta \mu| \end{aligned} \tag{51}$$

Substituting (51) into (50) yields:

$$\begin{aligned} \dot{V} \leq & - \left(k_1 - \frac{k_x}{2}\right) \hat{x}_e^2 - \left(c_1 - \frac{k_y}{2}\right) \hat{y}_e^2 - \frac{1}{2} (\lambda_3 - 2\ell_\zeta \lambda_2) \|E_\Omega\|^2 \\ & - \frac{\kappa_1}{2} \|\hat{W}^T - W^T\|^2 - \frac{\kappa_2}{2} (\hat{\vartheta} - \vartheta)^2 - (\omega_1^2 - 1) \tilde{d}^2 - \left(K_\Theta - \frac{1}{2} - \frac{K_n}{2}\right) \Theta^2 \\ & + (b - 1) |\Psi_3 \Delta \mu| + \frac{K_n}{2} |\Psi_4|^2 + \frac{\|\tilde{W}^T S\|^2}{2} + \frac{\tilde{\varepsilon}^2}{2} + \frac{\kappa_1}{2} \|W - W_0\|^2 \\ & + \frac{\kappa_2}{2} (\vartheta - \vartheta_0)^2 + \frac{k_x}{2} \hat{x}_e^2 + \frac{k_y}{2} \hat{y}_e^2 \\ \leq & -2\Xi_1 V + \Lambda_1 \end{aligned} \tag{52}$$

where $\Xi_1 = \min \left\{ k_1 - \frac{k_x}{2}, c_1 - \frac{k_y}{2}, \frac{1}{2} (\lambda_3 - 2\ell_\zeta \lambda_2), \frac{\kappa_1}{2}, \frac{\kappa_2}{2}, \omega_1^2 - 1, K_\Theta - \frac{1}{2} - \frac{K_n}{2} \right\}$, $\Lambda_1 = (b - 1) |\Psi_3 \Delta \mu| + \frac{K_n}{2} |\Psi_4|^2 + \frac{\|\tilde{W}^T S\|^2}{2} + \frac{\tilde{\varepsilon}^2}{2} + \frac{\kappa_1}{2} \|W - W_0\|^2 + \frac{\kappa_2}{2} (\vartheta - \vartheta_0)^2 + \frac{k_x}{2} \hat{x}_e^2 + \frac{k_y}{2} \hat{y}_e^2$.

When $|\Theta| < \chi_1$, note the following fact:

$$\begin{aligned} \Theta \dot{\Theta} &= 0 \\ \frac{K_n}{2} \Theta^2 &\leq -\frac{K_n}{2} \Theta^2 + K_n \chi_1^2 \\ \Psi_4 \Delta \mu &\leq \frac{1}{2} |\Psi_4|^2 + \frac{1}{2} \Delta \mu^2 \end{aligned} \tag{53}$$

Substituting (53) into (50) yields:

$$\begin{aligned} \dot{V} \leq & - \left(k_1 - \frac{k_x}{2}\right) \hat{x}_e^2 - \left(c_1 - \frac{k_y}{2}\right) \hat{y}_e^2 - \frac{1}{2} (\lambda_3 - 2\ell_\zeta \lambda_2) \|E_\Omega\|^2 \\ & - \frac{\kappa_1}{2} \|\hat{W}^T - W^T\|^2 - \frac{\kappa_2}{2} (\hat{\vartheta} - \vartheta)^2 - (\omega_1^2 - 1) \tilde{d}^2 - \frac{K_n}{2} \Theta^2 + \frac{1}{2} \Delta \mu^2 \\ & + \frac{1}{2} (K_n + 1) |\Psi_4|^2 + K_n \chi_1^2 + \frac{\|\tilde{W}^T S\|^2}{2} + \frac{\tilde{\varepsilon}^2}{2} + \frac{\kappa_1}{2} \|W - W_0\|^2 \\ & + \frac{\kappa_2}{2} (\vartheta - \vartheta_0)^2 + \frac{k_x}{2} \hat{x}_e^2 + \frac{k_y}{2} \hat{y}_e^2 \\ \leq & -2\Xi_2 V + \Lambda_2 \end{aligned} \tag{54}$$

where $\Xi_2 = \min \left\{ k_1 - \frac{k_x}{2}, c_1 - \frac{k_y}{2}, \frac{1}{2} (\lambda_3 - 2\ell_\zeta \lambda_2), \frac{\kappa_1}{2}, \frac{\kappa_2}{2}, \omega_1^2 - 1, \frac{K_n}{2} \right\}$, $\Lambda_2 = \frac{1}{2} \Delta \mu^2 + \frac{1}{2} (K_n + 1) |\Psi_4|^2 + K_n \chi_1^2 + \frac{\|\tilde{W}^T S\|^2}{2} + \frac{\tilde{\varepsilon}^2}{2} + \frac{\kappa_1}{2} \|W - W_0\|^2 + \frac{\kappa_2}{2} (\vartheta - \vartheta_0)^2 + \frac{k_x}{2} \hat{x}_e^2 + \frac{k_y}{2} \hat{y}_e^2$.

From (52) and (54), we have:

$$\dot{V} \leq -2\Xi V + \Lambda \tag{55}$$

where $\Xi = \min \{ \Xi_1, \Xi_2 \}$, $\Lambda = \max \{ \Lambda_1, \Lambda_2 \}$, and the selected parameters satisfy: $\lambda_3 > 2\ell_\zeta \lambda_2$, $\omega_1^2 > 1$, $K_\Theta > \frac{1}{2} + \frac{K_n}{2}$, $b > 1$.

Solving (55), we have:

$$V \leq \left(V(0) - \frac{\Lambda}{2\Xi} \right) e^{-2\Xi t} + \frac{\Lambda}{2\Xi} \tag{56}$$

Hence, we know that V is bounded by $\frac{\Lambda}{2\Xi}$, and all errors are guaranteed to be UUB. \square

5. Numerical Simulations

In this section, we conduct simulation studies using the MATLAB/Simulink environment. Meanwhile, two cases are applied to evaluate the performance of the proposed strategy, and the simulation results are compared with PLOS [13], the backstepping adaptive method [39], and the PID method. In addition, the following root mean squared error (RMSE) and mean integral absolute (MIA) value describing the error $\pi_e(\tau)$ are considered:

$$RMSE = \sum_{i=1}^N \sqrt{\frac{|\pi_e(\tau)|^2}{N}} \tag{57}$$

$$MIA = \frac{1}{t_\infty - t_0} \int_{t_0}^{t_\infty} |\pi_e(\tau)| d\tau$$

where N is the number of simulation steps.

The parameters of the USV can be obtained by [29], and the initial value is $[x, y, \psi]^T = [0, 2, 0]^T$, $[u, v, r]^T = [1, 0, 0]^T$. The design parameters are chosen as follows: $Q(t) = 0.5I_{4 \times 4}$, $k_x = 3$, $k_y = 2$, $k_1 = 8$, $\gamma = 5$, $\Delta_{\max} = 6$, $\Delta_{\min} = 2$, $R_1 = 0.06$, $h_1 = 0.02$, $\sigma_1 = 10$, $\kappa_1 = 2$, $\sigma_2 = 0.001$, $\kappa_2 = 0.02$, $\omega_j = 1.5 (j = 1, 2)$, $\omega_1 = 10$, $K_\Theta = 2$, $\chi_1 = 0.1$, $K_n = 3$. The desired path is chosen as $[x_d, y_d]^T = [10 \sin(0.1\theta) + 1.1\theta, \theta]^T$. In addition, the unmodeled dynamics and the time-varying external disturbances are selected as $\Delta f = 0.3f(r)$, $d(t) = 0.8 + 0.4 \sin(0.1t) + 0.3 \cos(0.2t)$, respectively.

Remark 4. It is worth noting that we can improve the control ability of the controller by choosing appropriate design parameters. For example: the bandwidth ω_j of enhanced TLC is selected by the pole assignment technique; R_1 of NTD is relatively sensitive. As R_1 becomes larger, the tracking speed becomes faster; as ω_1 of LESO increases, the error \tilde{d} will become smaller. Therefore, we should choose the parameters according to the actual situation.

Case 1. To verify the performance of the FPLOS guidance law, a comparison simulation is conducted between FPLOS and PLOS under the same design parameters.

Simulation results are provided in Figures 5–10, and the performance indices are reported in Table 1. Figure 5 shows that the designed FPLOS provides faster convergence speed and tracking performance than PLOS. The control inputs are given in Figure 6, and it is noted that the rudder saturation problem was effectively compensated by the auxiliary system. Figure 7 depicts that the actual heading could accurately track the desired heading using the designed FPLOS. Figure 8 depicts that the predictor was capable of identifying unknown sideslip angle. The errors x_e and y_e are shown in Figures 9 and 10. It can be seen from Figure 10 that y_e had fast convergence performance using the proposed FPLOS. The main reason was that the lookahead distance Δ was optimized reasonably by the fuzzy algorithm, thus achieving better convergence quality. It is shown from Table 1 that the RMSE and MIA values of FPLOS were [0.04941, 0.3473, 0.06539], [0.03204, 0.176, 0.0139], respectively, and they were only [9.42%, 53.3%, 87%] and [74.7%, 33.65%, 30.01%] of PLOS. Therefore, the designed FPLOS had better performance in terms of the convergence and stability.

Table 1. Performance comparisons of different methods. MIA, mean integral absolute. FPLOS, fuzzy predictor line-of-sight.

Method	Value					
	RMSE (x_e)	RMSE (y_e)	RMSE (E_1)	MIA (x_e)	MIA (y_e)	MIA (E_1)
TLC + FPLOS	0.04941	0.3473	0.06539	0.03204	0.176	0.0139
TLC + PLOS	0.5242	0.6508	0.07489	0.04284	0.523	0.04631

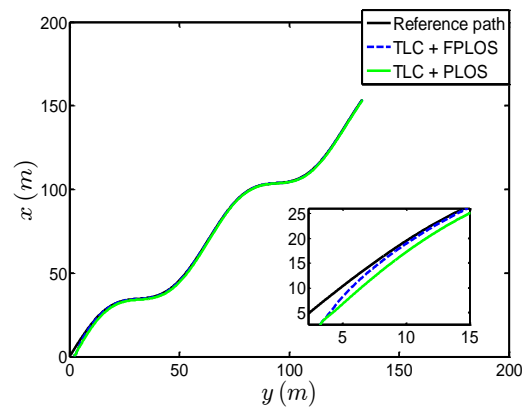


Figure 5. Path following performance.

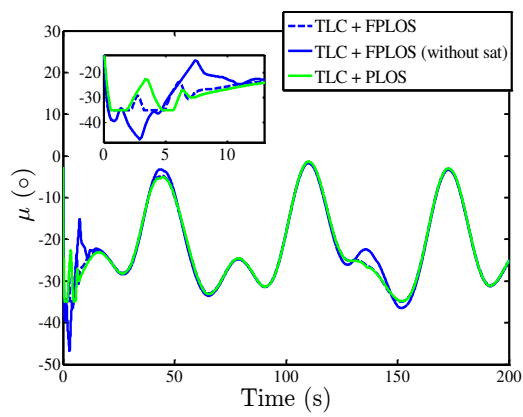


Figure 6. Control inputs μ .

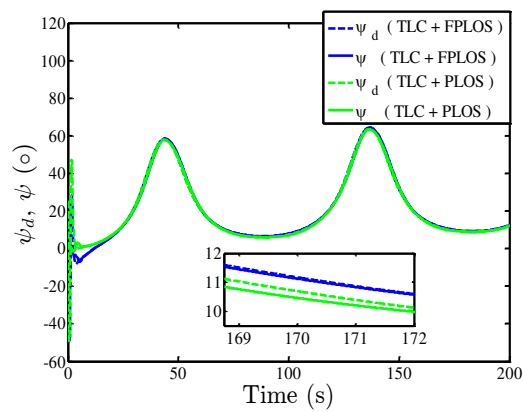


Figure 7. Guidance heading ψ_d and heading ψ .

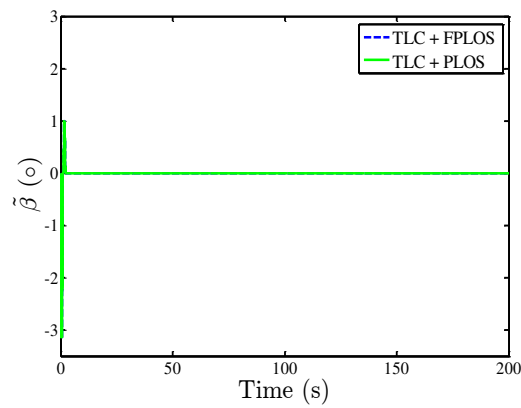


Figure 8. Sideslip angle estimation errors $\tilde{\beta}$.

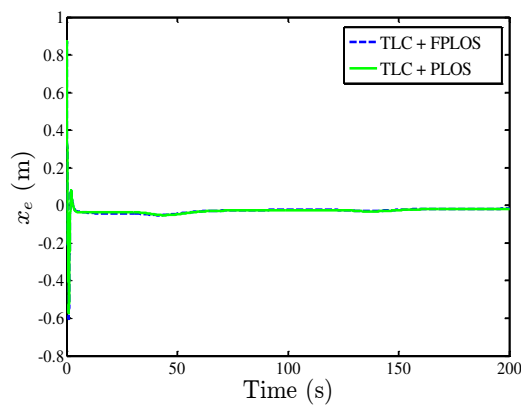


Figure 9. Along-track errors x_e .

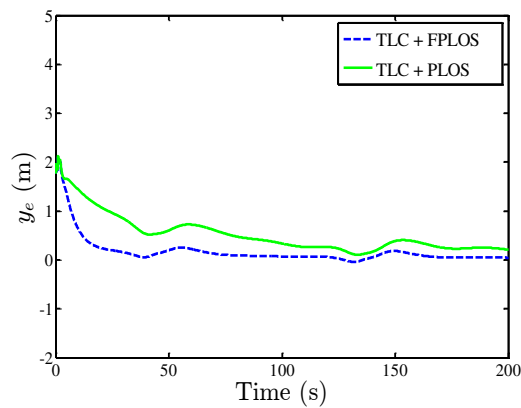


Figure 10. Cross-track errors y_e .

Case 2. Under the same condition and design parameters as Case 1, to prove the effectiveness of the designed TLC method, we provide a comparative simulation in TLC, backstepping, and the PID method.

Simulation results are displayed in Figures 11–16, and the performance indices are summarized in Table 2. Figure 11 presents the comparisons of the control performance, from which we can find that the designed TLC method exhibited better convergence performance than backstepping and the PID method even though being perturbed by unknown dynamics and external disturbances. Figure 12 depicts that the calculated control input exceeded the operation condition of the actuators, thus causing the problem of rudder saturation. It can also be seen from Figure 12 that an auxiliary system was incorporated into the proposed controller to handle this problem. Figure 13 shows that the actual heading could track

the guidance heading with arbitrarily small error. Figure 14 demonstrates sideslip angle estimation errors, and it can be clearly observed that the predictor could accurately estimate unknown sideslip angle. Figures 15 and 16 illustrate the tracking errors of the three control methods. It was evident that the errors of the designed TLC method could quickly converge to a small region around the origin. However, the errors of backstepping and PID were still fluctuating. Table 2 summarizes the comparison of the RMSE and MIA values of the three methods. It can be easily seen that the designed TLC method had higher tracking precision. All results demonstrated that our proposed control strategy exhibited superior control performance.

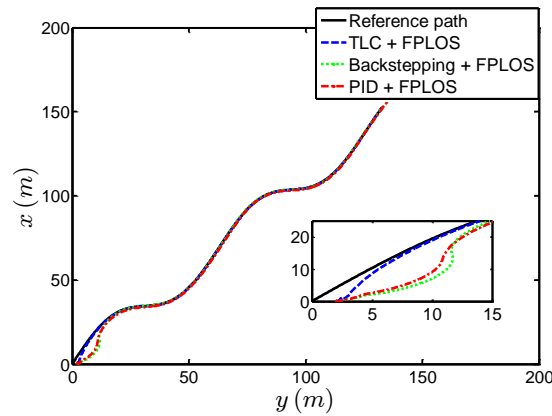


Figure 11. Path following performance.

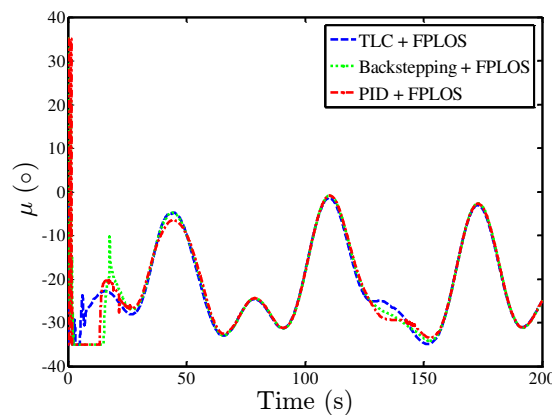


Figure 12. Control inputs μ .

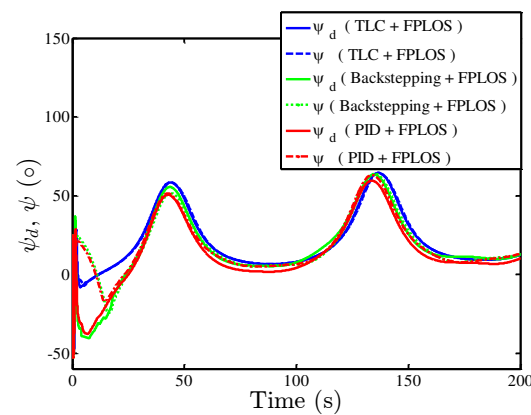


Figure 13. Guidance heading ψ_d and heading ψ .

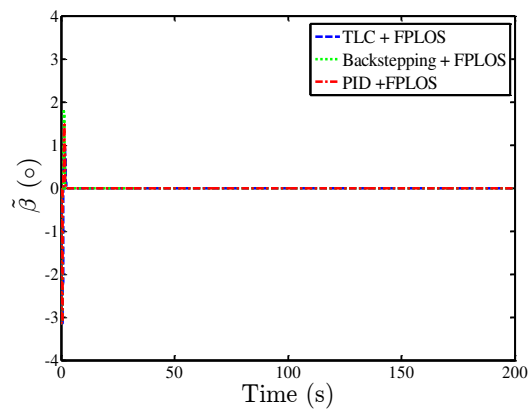


Figure 14. Sideslip angle estimation errors $\tilde{\beta}$.

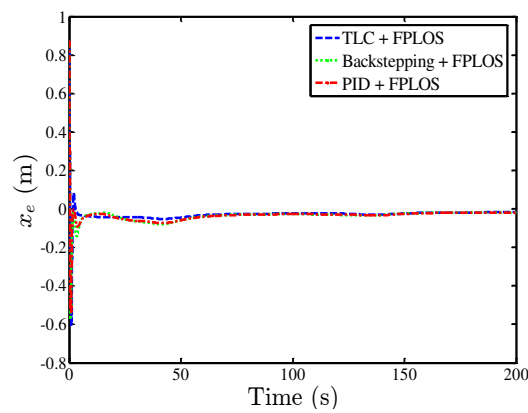


Figure 15. Along-track errors x_e .

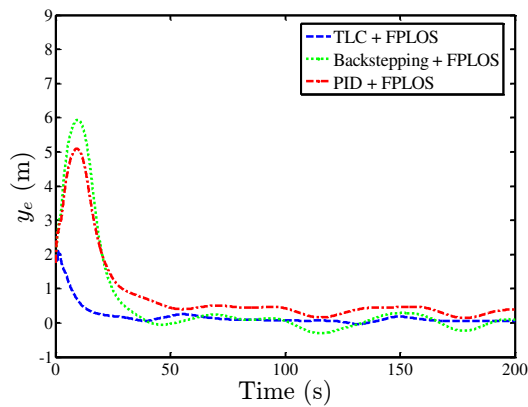


Figure 16. Cross-track errors y_e .

Table 2. Performance comparisons of different methods.

Method	Value					
	$RMSE(x_e)$	$RMSE(y_e)$	$RMSE(E_1)$	$MIA(x_e)$	$MIA(y_e)$	$MIA(E_1)$
TLC + FPLOS	0.04941	0.3473	0.06539	0.03204	0.176	0.0139
Backstepping + FPLOS	0.05564	1.501	0.2142	0.03753	0.6259	0.08243
PID + FPLOS	0.0549	1.354	0.191	0.0376	0.797	0.0864

6. Conclusions

In this paper, a novel path following control strategy was proposed for a USV subject to unmodeled dynamics, external disturbance, and rudder saturation. First, an FPLOS guidance strategy was developed to provide the guidance heading, which could also handle unknown sideslip angle. More importantly, the greatest advantage was that TLC was used as a new effective technique to design a concise path following controller, and the proposed controller could not only estimate and compensate for unknown dynamics and rudder saturation, but also provide high tracking precision. Meanwhile, NTD was applied in the proposed strategy to avoid unnecessary set-point jump. The superiority and the effectiveness of the proposed strategy were also confirmed by comparisons and extensive simulations. In the future, we will further optimize the lookahead distance using other methods [40–44], and the proposed design methods could also be used to solve the trajectory tracking problem of the USV and underwater vehicle.

Author Contributions: The work presented here was performed with the collaboration of all authors. Writing, review and editing, B.Q.; supervision, G.W.; funding acquisition, Y.F. All authors read and agreed to the published version of the manuscript.

Funding: This research was supported by the National Natural Science Foundation of China under Grant 51609033, the Natural Science Foundation of Liaoning Province under Grant 20180520005, the Key Development Guidance Program of Liaoning Province of China under Grant 2019JH8/10100100, the Soft Science Research Program of Dalian City of China under Grant 2019J11CY014, and the Fundamental Research Funds for the Central Universities under Grants 3132019005 and 3132019311.

Conflicts of Interest: The authors declare no conflict of interest.

Abbreviations

The following abbreviations are used in this manuscript:

USV	unmanned surface vehicle
TLC	trajectory linearization control
LESO	linear extended state observer
DSC	dynamic surface control
LOS	line-of-sight
PLOS	predictor line-of-sight
RBFNN	radial basis function neural network
NTD	nonlinear tracking differentiator
LTV	linear time-varying
UUB	uniformly ultimately bounded

References

1. Liu, Y.C.; Bucknall, R. Efficient multi-task allocation and path planning for unmanned surface vehicle in support of ocean operations. *Neurocomputing* **2018**, *275*, 142–149. [[CrossRef](#)]
2. Song, R.; Liu, Y.; Bucknall, R. A multi-layered fast marching method for unmanned surface vehicle path planning in a time-variant maritime environment. *Ocean Eng.* **2018**, *129*, 301–317. [[CrossRef](#)]
3. Zhao, Y.X.; Li, W.; Shi, P. A real-time collision avoidance learning system for Unmanned Surface Vessels. *Neurocomputing* **2016**, *182*, 255–266. [[CrossRef](#)]
4. Liu, L.; Wang, D.; Peng, Z.H. Path following of marine surface vehicles with dynamical uncertainty and time-varying ocean disturbances. *Neurocomputing* **2016**, *173*, 799–808. [[CrossRef](#)]
5. Oh, S.R.; Sun, J. Path following of underactuated marine surface vessels using line-of-sight based model predictive control. *Ocean Eng.* **2010**, *3*, 289–295. [[CrossRef](#)]
6. Peymani, E.; Fossen, T.I. Path following of underwater robots using Lagrange multipliers. *Robot. Auton. Syst.* **2015**, *67*, 44–52. [[CrossRef](#)]
7. Zheng, Z.W.; Sun, L. Path following control for marine surface vessel with uncertainties and input saturation. *Neurocomputing* **2016**, *177*, 158–167. [[CrossRef](#)]

8. Zhang, G.Q.; Zhang, X.K.; Zheng, Y.F. Adaptive neural path-following control for underactuated ships in fields of marine practice. *Ocean Eng.* **2015**, *104*, 558–567. [[CrossRef](#)]
9. Paliotta, C.; Lefeber, E.; Pettersen, K.Y.; Pinto, J.; Costa, M. Trajectory Tracking and Path Following for Underactuated Marine Vehicles. *IEEE Trans. Control Syst. Technol.* **2019**, *27*, 1423–1437. [[CrossRef](#)]
10. Fossen, T.I.; Lekkas, A.M. Direct and indirect adaptive integral line-of-sight path-following controllers for marine craft exposed to ocean currents. *Int. J. Adapt. Control Signal Process.* **2017**, *31*, 445–463. [[CrossRef](#)]
11. Zheng, Z.; Sun, L.; Xie, L.H. Error-Constrained LOS Path Following of a Surface Vessel with Actuator Saturation and Faults. *IEEE Trans. Syst. Man Cybern. Syst.* **2018**, *48*, 1794–1805. [[CrossRef](#)]
12. Wang, N.; Sun, Z.; Yin, J.C.; Su, S.F.; Sharma, S. Finite-Time Observer Based Guidance and Control of Underactuated Surface Vehicles with Unknown Sideslip Angles and Disturbances. *IEEE Access* **2018**, *6*, 14059–14070. [[CrossRef](#)]
13. Liu, L.; Wang, D.; Peng, Z.H.; Wang, H. Predictor-based LOS guidance law for path following of underactuated marine surface vehicles with sideslip compensation. *Ocean Eng.* **2016**, *124*, 340–348. [[CrossRef](#)]
14. Lekkas, A.M.; Fossen, T.I. Integral LOS path following for curved paths based on a monotone cubic Hermite spline parametrization. *IEEE Trans. Control Syst. Technol.* **2014**, *22*, 2287–2301. [[CrossRef](#)]
15. Liu, L.; Wang, D.; Peng, Z.H. ESO-Based Line-of-Sight Guidance Law for Path Following of Underactuated Marine Surface Vehicles with Exact Sideslip Compensation. *IEEE J. Ocean. Eng.* **2017**, *42*, 477–487. [[CrossRef](#)]
16. Wang, N.; Sun, Z.; Zheng, Z.; Zhao, H. Finite-Time Sideslip Observer-Based Adaptive Fuzzy Path-Following Control of Underactuated Marine Vehicles with Time-Varying Large Sideslip. *Int. J. Fuzzy Syst.* **2018**, *20*, 1767–1778. [[CrossRef](#)]
17. Fossen, T.I.; Pettersen, K.Y.; Galeazzi, R. Line-of-sight path following for dubins paths with adaptive sideslip compensation of drift forces. *IEEE Trans. Control Syst. Technol.* **2015**, *23*, 820–827. [[CrossRef](#)]
18. Peng, Z.; Wang, J.; Wang, D. Distributed Maneuvering of Autonomous Surface Vehicles Based on Neurodynamic Optimization and Fuzzy Approximation. *IEEE Trans. Control Syst. Technol.* **2017**, *99*, 1–8. [[CrossRef](#)]
19. Wang, N.; Meng, J.E. Direct Adaptive Fuzzy Tracking Control of Marine Vehicles With Fully Unknown Parametric Dynamics and Uncertainties. *IEEE Trans. Control Syst. Technol.* **2016**, *24*, 1845–1852. [[CrossRef](#)]
20. Mu, D.; Wang, G.; Fan, Y.; Sun, X.; Qiu, B. Adaptive LOS Path Following for a Podded Propulsion Unmanned Surface Vehicle with Uncertainty of Model and Actuator Saturation. *Appl. Sci.* **2017**, *7*, 1232. [[CrossRef](#)]
21. Shao, X.; Wang, H. Active disturbance rejection based trajectory linearization control for hypersonic reentry vehicle with bounded uncertainties. *ISA Trans.* **2015**, *54*, 27–38. [[CrossRef](#)] [[PubMed](#)]
22. Shao, X.; Wang, H. Back-stepping robust trajectory linearization control for hypersonic reentry vehicle via novel tracking differentiator. *J. Frankl. Inst.* **2016**, *353*, 1957–1984. [[CrossRef](#)]
23. Wang, N.; Er, M.J.; Sun, J.C.; Liu, Y.C. Adaptive Robust Online Constructive Fuzzy Control of a Complex Surface Vehicle System. *IEEE Trans. Cybern.* **2016**, *46*, 1511–1523. [[CrossRef](#)] [[PubMed](#)]
24. He, W.; Dong, Y.; Sun, C. Adaptive Neural Impedance Control of a Robotic Manipulator With Input Saturation. *IEEE Trans. Syst. Man Cybern. Syst.* **2017**, *46*, 334–344. [[CrossRef](#)]
25. Yu, Y.; Guo, C.; Yu, H. Finite-time predictor line-of-sight-based adaptive neural network path following for unmanned surface vessels with unknown dynamics and input saturation. *Int. J. Adv. Robot. Syst.* **2018**, *15*. [[CrossRef](#)]
26. Zheng, Z.; Feroskhan, M. Path Following of a Surface Vessel With Prescribed Performance in the Presence of Input Saturation and External Disturbances. *ASME Trans. Mechatron.* **2017**, *22*, 2564–2575. [[CrossRef](#)]
27. Du, J.; Hu, X.; Sun, Y. Adaptive Robust Nonlinear Control Design for Course Tracking of Ships Subject to External Disturbances and Input Saturation. *IEEE Trans. Syst. Man Cybern. Syst.* **2020**, *50*, 193–202. [[CrossRef](#)]
28. Zhu, G.; Du, J. Global Robust Adaptive Trajectory Tracking Control for Surface Ships Under Input Saturation. *IEEE J. Ocean. Eng.* **2018**, *45*, 442–450. [[CrossRef](#)]
29. Mu, D.; Wang, F.; Fan, Y.; Qiu, B.; Sun, X. Adaptive course control based on trajectory linearization control for unmanned surface vehicle with unmodeled dynamics and input saturation. *Neurocomputing* **2019**, *330*, 1–10. [[CrossRef](#)]
30. Breivik, M.; Hovstein, V.E.; Fossen, T.I. Straight-line target tracking for unmanned surface vehicles. *Model. Identif. Control* **2008**, *29*, 131–149. [[CrossRef](#)]
31. Khalil, H.K. *Nonlinear Systems*; Prentice Hall: New York, NY, USA, 1996.

32. Mickle, M.C.; Zhu, J.J. Skid to turn control of the APKWS missile using trajectory linearization technique. In Proceedings of the 2001 American Control Conference, Arlington, VA, USA, 25–27 June 2001; Volume 5, pp. 3346–3351.
33. Zhu, B.; Huo, W. Adaptive Trajectory Linearization Control for a model-scaled helicopter with uncertain inertial parameters. In Proceedings of the 31st Chinese Control Conference, Hefei, China, 25–27 July 2012; Volume 5, pp. 4389–4395.
34. Adami, T.M.; Zhu, J. 6DOF flight control of fixed-wing aircraft by Trajectory Linearization. In Proceedings of the 2011 American Control Conference, San Francisco, CA, USA, 29 June–1 July 2011; pp. 1610–1617.
35. Chen, Y.; Zhu, J. Car-like ground vehicle trajectory tracking by using trajectory linearization control. In Proceedings of the ASME 2017 Dynamic Systems and Control Conference, Tysons, VA, USA, 11–13 October 2017; Volume 2.
36. Huang, J.T. Global tracking control of strict-feedback systems using neural networks. *IEEE Trans. Neural Netw. Learn. Syst.* **2012**, *23*, 1714–1725. [[CrossRef](#)] [[PubMed](#)]
37. Han, J. From PID to active disturbance rejection control. *IEEE Trans. Ind. Electron.* **2009**, *56*, 900–906. [[CrossRef](#)]
38. Qiu, B.; Wang, G.; Fan, Y. Robust Adaptive Trajectory Linearization Control for Tracking Control of Surface Vessels with Modeling Uncertainties under Input Saturation. *IEEE Access* **2019**, *7*, 5057–5070. [[CrossRef](#)]
39. Lin, Y.; Du, J.; Niu, J. Design of Backstepping based adaptive robust nonlinear controller of ship course. *Ship Eng.* **2007**, *29*, 24–27.
40. Guerra, E.H.; Quiza, R.; Villalonga, A.; Arenas, J.; Castano, F. Digital Twin-Based Optimization for Ultraprecision Motion Systems with Backlash and Friction. *IEEE Access* **2019**, *7*, 93462–93472. [[CrossRef](#)]
41. Beruvides, G.; Juanes, C.; Castano, F.; Haber, R.E. A self-learning strategy for artificial cognitive control systems. In Proceedings of the 2015 IEEE 13th International Conference on Industrial Informatics (INDIN), Cambridge, UK, 22–24 July 2015; pp. 1180–1185.
42. Martin, A.G.; Guerra, E.H. Internal model control based on a neurofuzzy system for network applications. A case study on the high-performance drilling process. *IEEE Trans. Autom. Sci. Eng.* **2009**, *6*, 367–372. [[CrossRef](#)]
43. Guerra, E.H.; Alique, A.; Alique, J.R. Tool wear prediction in milling using neural networks. *Lect. Notes Comput. Sci.* **2002**, *2415*, 807–812.
44. Ebrahimi, Z.; Shahabi, H.; Soltani, M. Reinforcement learning for optimal scheduling of Glioblastoma treatment with Temozolomide. *Comput. Methods Programs Biomed.* **2020**, *193*, 105443. [[CrossRef](#)]



© 2020 by the authors. Licensee MDPI, Basel, Switzerland. This article is an open access article distributed under the terms and conditions of the Creative Commons Attribution (CC BY) license (<http://creativecommons.org/licenses/by/4.0/>).